THE JOURNAL OF BIOLOGICAL CHEMISTRY VOL. 286, NO. 49, pp. 42316–42324, December 9, 2011


# PRL-1 Protein Promotes ERK1/2 and RhoA Protein Activation through a Non-canonical Interaction with the Src Homology 3 Domain of p115 Rho GTPase-activating Protein*

Received for publication, July 25, 2011, and in revised form, October 17, 2011 Published, JBC Papers in Press, October 18, 2011, DOI 10.1074/jbc.M111.286302

**Yunpeng Bai**[‡1], **Yong Luo**[‡1], **Sijiu Liu**[‡], **Lujuan Zhang**[‡], **Kui Shen**[§], **Yuanshu Dong**[‡], **Chad D. Walls**[‡], **Lawrence A. Quilliam**[‡], **Clark D. Wells**[‡], **Youjia Cao**[¶], **and Zhong-Yin Zhang**[‡2]

*From the* [‡]*Department of Biochemistry and Molecular Biology, Indiana University School of Medicine, Indianapolis, Indiana 46202, the* [§]*Department of Chemistry and Biochemistry, Northern Illinois University, DeKalb, Illinois 60115, and the* [¶]*College of Life Sciences, Nankai University, Tianjin 300071, China*

**Background:** The mechanism for the oncogenic phosphatase PRL-1 remains undefined.
**Results:** We identified and characterized a novel PRL-1-binding protein, p115 RhoGAP.
**Conclusion:** PRL-1 activates the ERK1/2 pathway by displacing MEKK1 from p115 RhoGAP and RhoA by preventing its interaction with p115 RhoGAP.
**Significance:** This study offers a novel strategy for anticancer therapeutics by blocking the interaction between PRL-1 and p115 RhoGAP.

**Phosphatases of the regenerating liver (PRL) play oncogenic roles in cancer development and metastasis. Although previous studies indicate that PRL-1 promotes cell growth and migration by activating both the ERK1/2 and RhoA pathways, the mechanism by which it activates these signaling events remains unclear. We have identified a PRL-1-binding peptide (Peptide 1) that shares high sequence identity with a conserved motif in the Src homology 3 (SH3) domain of p115 Rho GTPase-activating protein (GAP). p115 RhoGAP directly binds PRL-1 *in vitro* and in cells via its SH3 domain. Structural analyses of the PRL-1·Peptide 1 complex revealed a novel protein-protein interaction whereby a sequence motif within the P*xx*P ligand-binding site of the p115 RhoGAP SH3 domain occupies a folded groove within PRL-1. This prevents the canonical interaction between the SH3 domain of p115 RhoGAP and MEKK1 and results in activation of ERK1/2. Furthermore, PRL-1 binding activates RhoA signaling by inhibiting the catalytic activity of p115 RhoGAP. The results demonstrate that PRL-1 binding to p115 RhoGAP provides a coordinated mechanism underlying ERK1/2 and RhoA activation.**

Phosphatases of the regenerating liver (PRL) represent a unique subfamily of protein-tyrosine phosphatases with three members (PRL-1, -2, and -3), sharing a high degree (>75%) of amino acid sequence identity (1–3). The PRL phosphatases possess a C-terminal prenylation motif, which is important for their localization to the plasma membrane and early endosomal compartments (2, 4, 5). Substantial evidence suggests a role for the PRL phosphatases in controlling cell growth and invasion (6–8).

PRL-1 was originally identified as an immediate-early gene whose expression was induced during liver regeneration after partial hepatectomy (1). Subsequently, PRL-1 expression was found to be elevated in many tumor cell lines, and cells expressing high levels of PRL-1 exhibit enhanced proliferation and anchorage-independent growth (1, 2, 5, 9). PRL-1 also promotes cell invasion and tumor metastasis. For example, CHO or HEK293 cells stably expressing PRL-1 display enhanced motility and invasiveness (3, 10). CHO cells with elevated PRL-1 also preferentially form metastatic tumors in nude mice (3). Furthermore, an increase in PRL-1 expression enhances motility and invasion of colon adenocarcinoma cells (11), whereas knockdown of endogenous PRL-1 inhibits human A549 lung cancer cell invasion (12). These results suggest an oncogenic role for PRL-1 in cancer development and metastatic progression.

Recent biochemical studies revealed that PRL-1 promotes cell proliferation and invasion by up-regulating both the ERK1/2 and RhoA pathways (10, 11, 13, 14). ERK1 and ERK2 are serine/threonine kinases that are required for many fundamental processes, including cell proliferation, survival, and motility (15), whereas the Rho family GTPases are recognized mainly as key regulators of actin cytoskeletal dynamics and cell migration (16, 17). However, the underlying mechanism by which PRL-1 activates ERK1/2 and RhoA remains to be established. In an effort to identify novel effectors of PRL-1, we screened a phage display library and identified a PRL-1-binding peptide that corresponds to a sequence motif within the Src homology 3 (SH3)[3] domain of p115 Rho GTPase-activating protein (GAP). Biochemical, cellular, and structural analyses revealed that p115 RhoGAP is a *bona fide* PRL-1-binding pro-

* This work was supported, in whole or in part, by National Institutes of Health Grants CA69202 and CA126937.
*The atomic coordinates and structure factors (code 3RZ2) have been deposited in the Protein Data Bank, Research Collaboratory for Structural Bioinformatics, Rutgers University, New Brunswick, NJ (http://www.rcsb.org/).*
[1] Both authors contributed equally to this work.
[2] To whom correspondence should be addressed. E-mail: zyzhang@iupui.edu.

[3] The abbreviations used are: SH3, Src homology 3; GAP, GTPase-activating protein; SrGAP, Slit-Robo GAP, BisTris, 2-[bis(2-hydroxyethyl)amino]-2-(hydroxymethyl)propane-1,3-diol.

tein. Importantly, the interaction between PRL-1 and p115 RhoGAP promotes ERK1/2 activation by displacing MEKK1 (MAPK/ERK kinase kinase 1) from its inhibitor p115 RhoGAP. Moreover, we provide evidence that PRL-1 activates RhoA by directly inhibiting the catalytic activity of p115 RhoGAP.

## EXPERIMENTAL PROCEDURES

*Materials*—Anti-HA, anti-His, anti-GST, anti-RhoA, anti-actin, and anti-MEKK1 antibodies were purchased from Santa Cruz Biotechnology. Anti-FLAG and anti-p115 RhoGAP antibodies were from Sigma. Anti-ERK1/2, anti-phospho-ERK1/2 (Thr-202/Tyr-204), and anti-Myc polyclonal antibodies were obtained from Cell Signaling (Beverly, MA). Anti-PRL-1 antibody was a generous gift from Dr. Qi Zeng. DMEM, fetal bovine serum, penicillin, and streptomycin were from Invitrogen.

*Phage Display*—The Ph.D.-12 phage display peptide library kit (New England Biolabs) is based on a combinatorial library of a random 12-mer peptide fused to a minor coat protein (PIII) of M13 phage. The titer of the library is $1.5 \times 10^{13}$ plaque-forming units. The library contains a complexity of $2.7 \times 10^9$ sequences. On day 1, 3 $\mu$g of recombinant PRL-1 was coated in a well of a 96-well plate at 4 °C overnight. On day 2, 200 $\mu$l of MPBS (2% (v/v) nonfat milk in PBS (137 mM NaCl, 2.7 mM KCl, 10 mM $NaH_2PO_4$, and 1.4 mM $KH_2PO_4$, pH 7.4)) was added to the well with shaking for 1 h at room temperature to block nonspecific binding. During this time, the input phage was mixed in 100 $\mu$l of MPBS and incubated for 1 h at room temperature in an empty well to allow any "sticky" phage to adhere to the plastic. The protein/MPBS solution was discarded, and the well was washed five times with 200 $\mu$l if PBST (0.1% (v/v) Tween in PBS). The phage/MPBS solution was transferred from the preclearing well to the PRL-1-coated well, followed by incubation for 2 h at room temperature with shaking. After washing away the unbound phage with 200 $\mu$l of PBST five times, the bound phage was eluted by the addition of 100 $\mu$l of 0.1 M HCl for 10 min at room temperature with shaking. The eluted phage was transferred to a tube and immediately neutralized by the addition of 50 $\mu$l of 1 M Tris-HCl buffer, pH 7.4. A small part of this output phage was used for titration, and the rest was amplified to obtain an input titer of $10^{13}$ phage for the following panning. A total of four rounds of panning were performed to obtain PRL-1-specific phage. Individual phage clones were amplified, and single-strand DNA was isolated according to the manufacturer's instructions. The sequence of the 12-amino acid PRL-1-binding peptide was obtained by DNA sequencing.

*Cell Culture and Transfection*—HEK293 cells and mouse embryonic fibroblast cells were grown in DMEM supplemented with 10% fetal bovine serum, 50 units/ml penicillin, and 50 $\mu$g/ml streptomycin under a humidified atmosphere containing 5% $CO_2$. HEK293 cells were seeded at 40% confluency in antibiotic-free medium and grown overnight. Transfection was performed using FuGENE 6 (Roche Applied Science) according to the manufacturer's recommendations.

*Immunoblotting and Immunoprecipitation*—Cells were grown to 70% confluency, washed with ice-cold PBS, and lysed on ice for 30 min in lysis buffer (50 mM Tris-HCl, pH 7.4, 150 mM NaCl, 1% Triton X-100, and 10% glycerol) supplemented with a Complete protease inhibitor tablet (Roche Applied Science). Cell lysates were cleared by centrifugation at 15,000 rpm for 10 min. The lysate protein concentration was estimated using a BCA protein assay kit (Pierce). For immunoprecipitation, 3 $\mu$g of antibody was added to 1 mg of cell lysate and incubated at 4 °C for 4 h with protein A/G-agarose beads. After being extensively washed, the protein complex was boiled with sample buffer, separated by SDS-PAGE, transferred electrophoretically to a nitrocellulose membrane, and immunoblotted with appropriate antibodies, followed by incubation with horseradish peroxidase-conjugated secondary antibodies. The blots were developed by the enhanced chemiluminescence technique (ECL kit, GE Healthcare). Representative results from at least two independent experiments are shown.

*GST Pulldown Assay*—Pulldown assays were performed with GST, GST-fused Peptide 1, or the GST-fused Slit-Robo GAP (SrGAP) SH3 domain bound to reduced glutathione-agarose after washing three times with Tris-buffered saline. Purified His-PRL-1 proteins or cell lysates containing HA-PRL-1 were added to immobilized GST fusion proteins in binding buffer (50 mM Tris-HCl, pH 7.5, 150 mM NaCl, 10% glycerol 0.5% Triton X-100, 5 mM EDTA, and proteinase inhibitor mixture) and incubated for 2 h at 4 °C in a tube rotator. After centrifugation, the beads were kept on ice and washed three times for 5 min each with wash buffer (50 mM Tris-HCl, pH 7.5, 150 mM NaCl, 10% glycerol, 0.1% Triton X-100, 5 mM EDTA, and proteinase inhibitor mixture). The washed beads were boiled in loading buffer for 5 min and separated on SDS-polyacrylamide gel. Proteins were transferred to PVDF and immunostained with anti-His, anti-HA, and anti-GST antibodies.

*Effector Pulldown Assay*—Effector pulldown assay was performed to monitor RhoA activity. Cells were lysed in buffer containing 20 mM Tris-HCl, pH 7.6, 100 mM NaCl, 1% Triton X-100, 10 mM $MgCl_2$, 2 mM NaF, and protease inhibitor mixture for 30 min at 4 °C. Cell lysate was incubated with the GST-fused Rho-binding domain of Rhotekin immobilized on reduced glutathione-agarose for 2 h at 4 °C in a tube rotator. The level of active RhoA was detected by Western blotting with anti-RhoA antibody.

*GAP Activity Assay*—Immunoprecipitated p115 RhoGAP activity was measured by analyzing the ratio of GTP and GDP bound to RhoA as described (18). Recombinant human RhoA protein was purified as described (19) and was loaded with [$\alpha$-$^{32}$P] GTP by incubation for 10 min at 30 °C in 50 mM Tris-HCl, pH 7.4, 150 mM NaCl, 5 mM EDTA, 1 mg/ml BSA, 6 $\mu$M GTP, 5 $\mu$Ci of [$\alpha$-$^{32}$P]GTP, and 1 mM dithiothreitol. $MgCl_2$ was added to 10 mM, and free nucleotide was removed by washing the beads three times with the loading buffer minus GTP. Proteins were then eluted by incubating the beads with 100 $\mu$l of 100 mM Tris-HCl, pH 8.0, 10 mM $MgCl_2$, and 20 mM glutathione on ice for 20 min. GTP-loaded RhoA was incubated with FLAG-p115 RhoGAP produced by transient transfection in 293 cells and immunoprecipitation with anti-FLAG antibody in a 50-$\mu$l final reaction volume containing 25 mM Tris-HCl, pH 7.5, 1.5 mg/ml BSA, 7.5 mM $MgCl_2$, and 2 mM dithiothreitol at room temperature for 1 h. The reaction was stopped by the addition of 4 $\mu$l of 0.5 M EDTA and 1 $\mu$l of 10% SDS; RhoA protein was denatured by incubation at 68 °C for 5 min; and guanine nucleotides were separated by thin layer chromatography on poly-

ethyleneimine-cellulose TLC plates (Mallinckrodt Baker) using 0.75 M $KH_2PO_4$/HCl, pH 3.4, as the solvent. Chromatograms were dried, and Ras-bound GDP and GTP were visualized by autoradiography.

*Immunofluorescence and Confocal Microscopy*—Mouse embryonic fibroblast cells were cultured directly on glass coverslips in 6-well plates. Twenty-four hours later, cells were transfected with the indicated constructs. After an additional 24 h, cells were fixed with 4% paraformaldehyde in PBS for 10 min at room temperature, permeabilized with 0.2% Triton X-100 in PBS for 10 min, and blocked with BSA. Monoclonal antibody to FLAG (M2) was applied for 1 h, followed by a 1-h incubation with Texas Red-conjugated anti-mouse immunoglobulin G (Jackson ImmunoResearch Laboratories). DNA staining (0.5 $\mu$g of Hoechst 33258/ml; Sigma) was used to identify cell nuclei. After being washed with PBS, the coverslips were mounted with antifade mounting solution. Confocal microscope images were obtained with a Zeiss Axio Observer.Z1 microscope with a Plan Apochromat ×63 oil immersion objective and processed with Zeiss AxioVision 4.7.

*Cell Migration Assay*—Cell migration was assessed as described previously (13) with some modifications. The assay was performed with Corning Transwells (6.5-mm diameter, 8-$\mu$m pore size polycarbonate membrane; Costar, Acton, MA). Cells ($3.75 \times 10^5$) in 1.5 ml of serum-free medium were placed in the upper chamber, whereas the lower chamber was loaded with 2.6 ml of medium containing 10% FBS. After incubation at 37 °C with 5% $CO_2$ for 24 h, the total numbers of cells that migrated into the lower chamber were counted with a hemocytometer.

*siRNA Knockdown*—Duplex siRNAs were provided by Proligo at a concentration of 50 $\mu$M. The siRNA sequences were as follows: human p115 RhoGAP-1, 5′-CUGAGGUGCCGCUGCUGGAdTdT (sense) and 5′-UCCAGCAGCGGCACCUCAGdTdT (antisense), target position 2880; and p115 RhoGAP-2, 5′-GCGUGAAUGCCGAGGCCAAdTdT (sense) and 5′-UUGGCCUCGGCAUUCACGCdTdT (antisense), target position 575. siRNAs were transfected by RNAiFect (Qiagen), and the knockdown of targeted genes was verified after 72 h by Western blot analysis.

*Luciferase Assay*—Luciferase assays were modified as described previously (13). Cells were transfected with the SRE.L triple-repeat promoter-luciferase construct (20). Cells were harvested and lysed 48 h after transfection. Luciferase activities were determined using the luciferase assay system (Promega) according to the manufacturer's specifications. Individual assays were normalized by internal *Renilla* luciferase activity. Experiments were performed in triplicate and repeated three times with similar results. The statistics were done using Student's *t* test, with $p < 0.05$ considered significant.

*Crystallization and Data Collection*—PRL-1 (7 mg/ml) was mixed with Peptide 1 at a molar ratio of 1:2, and PRL-1·Peptide 1 was co-crystallized by vapor diffusion in hanging drops at 4 °C. Drops containing 1:1 volumes of the protein in stock buffer (20 mM Tris-HCl, pH 7.5) and reservoir solution A (20% PEG 3350, 0.1 M NaCl, and 0.1 M BisTris, pH 6.4) were equilibrated against reservoir solution A. The crystal was transferred into reservoir solution B (28% PEG 3350, 0.1 M NaCl, 0.1 M BisTris, pH 6.4, and 0.2 mM Peptide 1), soaked for 5 h, and flash-cooled in liquid nitrogen. X-ray data were collected at 100 K at Structural Biology Center Collaborative Access Team beamline 19-BM (Advanced Photon Source, Argonne, IL) equipped with a mosaic CCD detector. All data were processed with HKL3000 (21), and the statistics are provided in Table 1.

*Structural Determination and Refinement*—The structure of PRL-1·Peptide 1 was solved by molecular replacement using the program AMoRe (22). The structure of PRL-1 (Protein Data Bank code 2ZCK) (23) without the solvent molecules was used as the search model. The structure was refined to 2.8 Å resolution with the program CNS1.1 (24). The progress of the refinement was evaluated by the improvement in the quality of the electron density maps and the reduced values of the conventional *R* factor and the free *R* factor (with 3.3% of the reflections omitted from the refinement) (25). Electron density maps were inspected, and the model was modified on an interactive graphics work station with the program O (26). Finally, water molecules were added gradually as the refinement progressed. They were assigned in the $F_o - F_c$ difference Fourier maps with a $3\sigma$ cutoff for inclusion in the model.

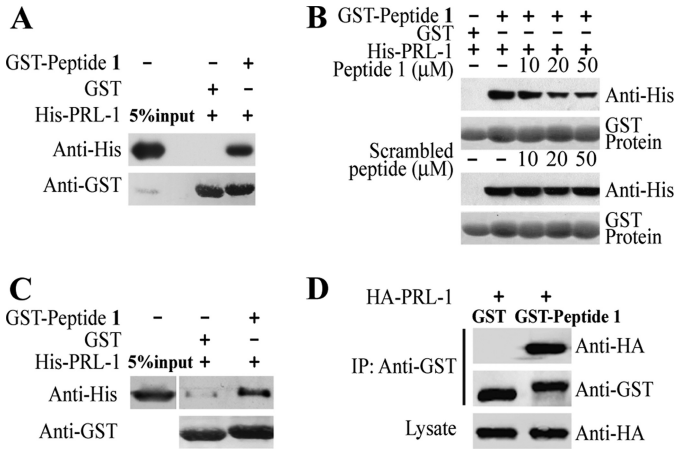


FIGURE 1. **Identification and characterization of a PRL-1-binding Peptide 1.** *A*, *in vitro* GST pulldown assay verified the interaction between $His_6$-tagged PRL-1 and GST-Peptide 1. *B*, synthetic Peptide 1 blocks binding between PRL-1 and GST-Peptide 1. *C*, GST-Peptide 1 pulls down HA-tagged PRL-1 from HEK293 cell lysate. *D*, GST-Peptide 1 co-immunoprecipitates (*IP*) HA-PRL-1 from HEK293 cells. Data shown are representative of triplicate experiments with similar results.

## RESULTS AND DISCUSSION

*Identification and Characterization of a PRL-1-binding Peptide*—We hypothesized that the discovery of PRL-1-binding proteins may yield new insight into the mechanism that accounts for PRL-1-mediated ERK1/2 and RhoA activation. Using recombinant PRL-1 protein, we screened a phage display 12-mer peptide library and identified Peptide 1 (GWWSLIPPKYIT) as a putative PRL-1-binding peptide. Consistent with this peptide interacting with PRL-1, purified GST-Peptide 1 fusion protein, but not GST, was capable of precipitating $His_6$-tagged recombinant PRL-1 from solution (Fig. 1*A*). The concentration-dependent displacement of PRL-1 from the GST-Peptide 1 fusion protein by synthetic Peptide 1, but not by a scrambled peptide, indicates the specificity of this interaction (Fig. 1*B*). In addition, GST-Peptide 1 pulled down HA-PRL-1

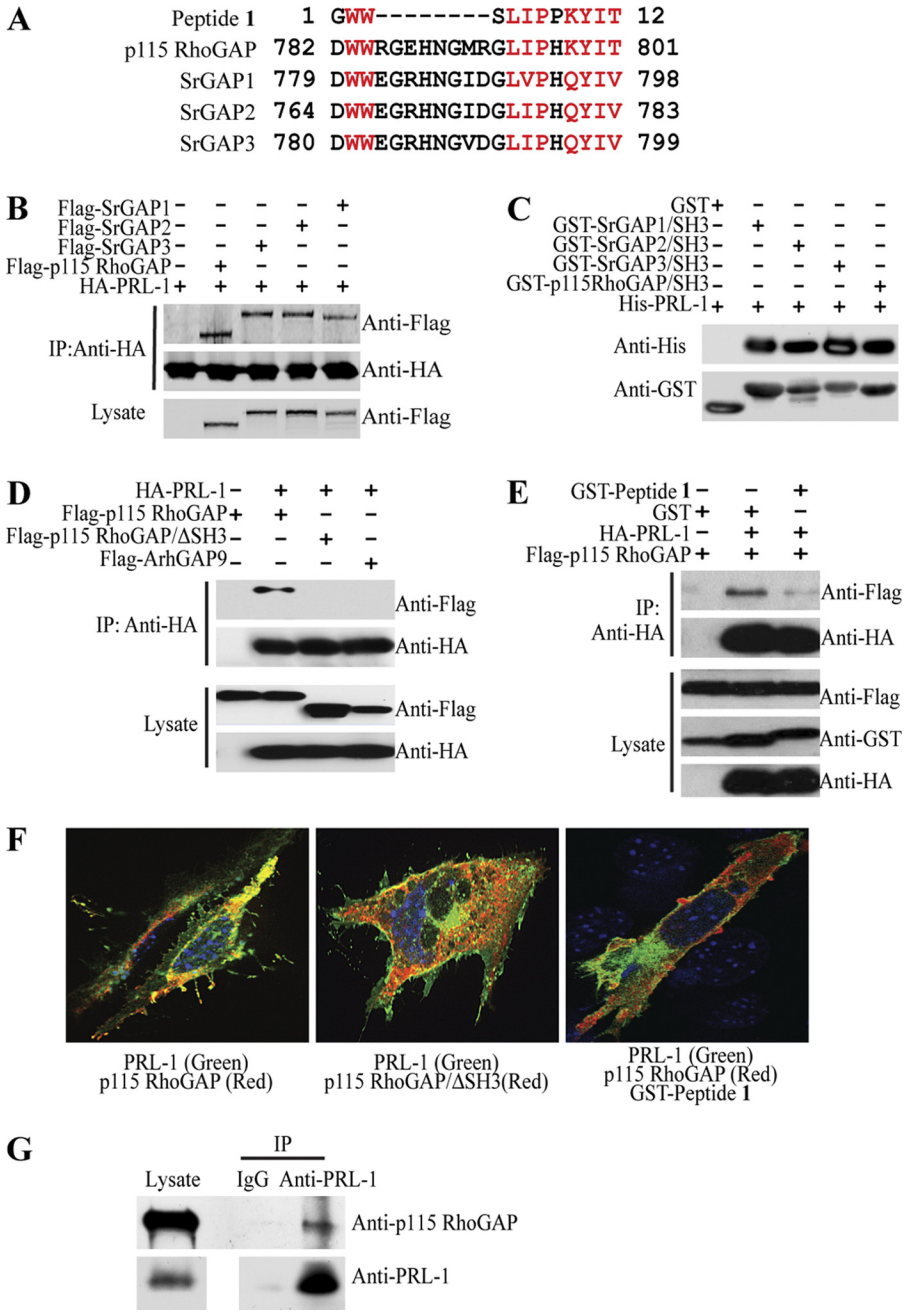


FIGURE 2. **Identification of p115 RhoGAP as a PRL-1-binding protein.** *A*, sequence alignment between Peptide 1 and p115 RhoGAP, SrGAP1, SrGAP2, and SrGAP3. *B*, HA-tagged PRL-1 immunoprecipitates (*IP*) p115 RhoGAP, SrGAP1, SrGAP2, and SrGAP3 from HEK293 cells. *C*, recombinant $His_6$-tagged PRL-1 binds the SH3 domains of p115 RhoGAP, SrGAP1, SrGAP2, and SrGAP3 in a GST pulldown assay. *D*, the interaction between PRL-1 and p115 RhoGAP depends on the SH3 domain of p115 RhoGAP. PRL-1-expressing HEK293 cells were transfected with FLAG-tagged full-length p115 RhoGAP, p115 RhoGAPΔSH3, and ArhGAP9. PRL-1 was immunoprecipitated with anti-HA antibody, and the immunoprecipitates were blotted with anti-FLAG antibody to detect the binding of p115 RhoGAP. *E*, GST-Peptide 1 disrupts the interaction between HA-PRL-1 and FLAG-p115 RhoGAP inside HEK293 cells. *F*, subcellular co-localization of PRL-1 and p115 RhoGAP in mouse embryonic fibroblast cells. Cells were processed for imaging within 24 h after transfection with GFP-PRL-1, FLAG-p115 RhoGAP, FLAG-p115 RhoGAPΔSH3, or GST-Peptide 1. p115 RhoGAP or p115 RhoGAPΔSH3 was detected by indirect immunostaining for the FLAG epitope (*red*). Nuclei were stained with Hoechst 33258 dye (*blue*), whereas GFP-PRL-1 (*green*) was directly visualized. The images from merging the three confocal fluorescence channels are depicted, where co-localization between *red* and *green* is seen as *yellow*. For each experiment, we analyzed at least 10 representative cells. Images of representative cells are shown. *G*, endogenous PRL-1 immunoprecipitates endogenous p115 RhoGAP in H1299 cells. The Western blot shown is representative of triplicate experiments with similar results.

from HEK293 cell lysate (Fig. 1*C*), and GST-Peptide 1 readily co-immunoprecipitated with HA-PRL-1 when both were expressed in HEK293 cells (Fig. 1*D*). Collectively, these results indicate that Peptide 1 directly binds PRL-1 both in solution and in mammalian cells.

*Identification of p115 RhoGAP as a PRL-1-binding Protein*—To identify PRL-1-binding proteins, we launched a BLAST search using Peptide 1 as a query. The top hit was the human protein p115 RhoGAP (27), a member of the SrGAP family of proteins that have attributed roles in axon guidance and cell

**TABLE 1**
**Crystallographic data and refinement statistics for the PRL-1·Peptide 1 complex**

| | |
|---|---|
| **Space group** | $I2_13$ |
| **Cell dimensions** | $a = 146.5, b = 146.5, c = 146.5$ Å |
| **Data collection** | |
| Resolution range (Å) | 50.0–2.5 |
| No. of unique reflections | 18,287 |
| Completeness (%) | 99.9 (99.8)[a] |
| Redundancy | 24.9 |
| $R_{merge}$[b] | 0.150 (0.872)[a] |
| **Refinement** | |
| Resolution range (Å) | 50.0–2.8 |
| No. of reflections used ($F \geq 1.5\delta(F)$) | 12,045 |
| No. of protein atoms | 2280 |
| No. of peptides | 2 |
| No. of waters | 38 |
| $R_{work}$[c]/$R_{free}$[d] | 18.0/20.1 |
| **r.m.s.d.[e] from ideal geometry** | |
| Bond length (Å) | 0.008 |
| Bond angle | 1.33° |
| **Average *B*-factors (Å$^2$)** | |
| Overall | 65.80 |
| Protein | 65.45 |
| Peptide 1 | 72.16 |
| Waters | 61.56 |

[a] The values in parentheses correspond to the highest resolution shell (2.54–2.50 Å).
[b] $R_{merge} = \Sigma_h\Sigma_i|I(h)_i - \langle I(h)\rangle|/\Sigma_h\Sigma_i I(h)_i$.
[c] $R_{work} = \Sigma_h|F(h)_{calc} - F(h)_{obs}|/\Sigma F(h)_{obs}$, where $F(h)_{calc}$ and $F(h)_{obs}$ are the refined calculated and observed structure factors, respectively.
[d] $R_{free}$ was calculated for a randomly selected 3.3% of the reflections that were omitted from refinement.
[e] r.m.s.d., root mean square deviation.

migration (28, 29). All members of the SrGAP family (SrGAP1, -2, and -3 and p115 RhoGAP) contain an N-terminal FCH (Fes/CIP4 (Cdc42-interacting protein 4) homology) domain and a central RhoGAP domain, which is followed by an SH3 domain (27, 30). Because Peptide 1 shares strong sequence identity with contiguous residues in the SH3 domains of all SrGAP proteins (Fig. 2*A*), we compared their relative association with PRL-1 by co-immunoprecipitation. For this purpose, FLAG-tagged p115 RhoGAP, SrGAP1, SrGAP2, and SrGAP3 were transfected into HEK293 cells stably expressing HA-PRL-1. Protein complexes were immunoisolated from cell lysates using anti-HA antibodies and immunoblotted with antibodies against FLAG and HA. This revealed that PRL-1 co-immunoprecipitated with all SrGAP family members (Fig. 2*B*). Consistently, GST pulldown assays demonstrated that PRL-1 could directly bind the SH3 domain of each SrGAP (Fig. 2*C*), but not a fragment of p115 RhoGAP lacking its SH3 domain or ArhGAP9, an SH3 domain-containing RhoGAP that is not in the SrGAP family (Fig. 2*D*). Furthermore, GST-Peptide 1 disrupted the intracellular association between PRL-1 and p115 RhoGAP (Fig. 2*E*). These findings suggest that PRL-1 binds p115 RhoGAP through a short motif in its SH3 domain.

We next examined the subcellular co-distribution of PRL-1 and p115 RhoGAP. FLAG-tagged p115 RhoGAP and GFP-tagged PRL-1 were coexpressed in mouse embryonic fibroblast cells, and their cellular localization was visualized by confocal immunofluorescence microscopy (Fig. 2*F*). Consistent with previous observations (4), PRL-1 was associated with the

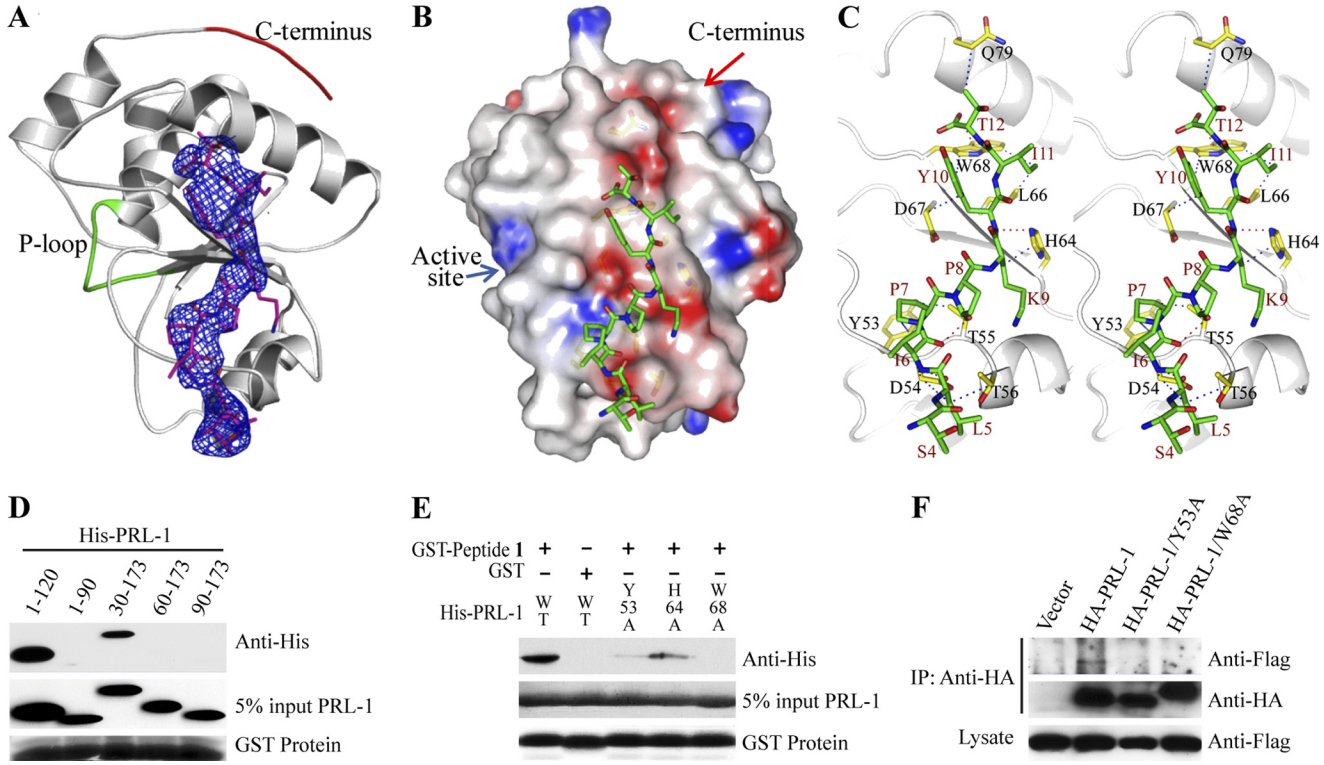


FIGURE 3. **Structural basis of PRL-1 interaction with Peptide 1 and the SH3 domain of p115 RhoGAP.** *A*, overall structure of PRL-1 in complex with Peptide 1. The peptide is shown in stick model with the unbiased omit $F_o - F_c$ density map contoured at 3.0$\sigma$. The P-loop and C terminus are shown in *green* and *red*, respectively. *B*, surface representation of PRL-1 in complex with Peptide 1, colored by electrostatic potential calculated by DelPhi. *C*, stereo diagram of the interactions between residues in PRL-1 (*yellow*) and Peptide 1 (*green*). *D*, identification of the region in PRL-1 responsible for binding p115 RhoGAP by GST pulldown assay. *E*, substitution of PRL-1 Tyr-53, His-64, and Trp-68 impairs its ability to bind GST-Peptide 1. *F*, substitution of PRL-1 Tyr-53 and Trp-68 abrogates its ability to bind p115 RhoGAP in HEK293 cells. Western blots shown are representative of triplicate experiments with similar results. *IP*, immunoprecipitate.

plasma membrane as well as with intracellular punctate structures dispersed throughout the cytoplasm. Similar to the earlier finding that p115 RhoGAP localizes to the leading edges of cells via the FCH domain (31), we observed that p115 RhoGAP resides primarily at the cell periphery, and this pattern of localization is independent of the SH3 domain. In agreement with our findings that p115 RhoGAP biochemically associates with PRL-1, these proteins highly co-localized at the plasma membrane and at the leading edges of cells. However, a mutant of p115 RhoGAP lacking the SH3 domain showed no co-localization with PRL-1. In addition, cotransfection of GST-Peptide 1 abrogated the co-localization of p115 RhoGAP and PRL-1. Taken together, these results support the conclusion that p115 RhoGAP is a specific PRL-1-binding protein and that a motif within the SH3 domain of p115 RhoGAP is required for binding PRL-1. We further suggest that Peptide 1 and a region within the SH3 domain of p115 RhoGAP bind a common site in PRL-1.

Finally, we determined whether PRL-1 can bind p115 RhoGAP under endogenous conditions. PRL-1 is overexpressed in many lung cancer cell lines, including H1299 cells (5). Knockdown of PRL-1 in H1299 cells significantly decreases cell proliferation and migration (13). To demonstrate direct association of PRL-1 and p115 RhoGAP in H1299 cells, we used anti-PRL-1 antibodies to immunoprecipitate endogenous PRL-1. As shown in Fig. 2*G*, we detected p115 RhoGAP in the PRL-1 immunoprecipitates, indicating endogenous association between PRL-1 and p115 RhoGAP.

*Structural Basis of PRL-1 Interaction with Peptide 1 and the SH3 Domain of p115 RhoGAP*—To elucidate the molecular basis by which PRL-1 recognizes Peptide 1 and most likely the SH3 domain of p115 RhoGAP, we solved the crystal structure of PRL-1 in complex with Peptide 1 at 2.8 Å resolution. Data collection and structural refinement statistics are summarized in Table 1. The final atomic model encompasses residues 9–160 of PRL-1 in a complex with residues 4–12 of Peptide 1, as revealed by the unbiased $F_o - F_c$ omit density map (Fig. 3*A*). Peptide 1 binds PRL-1 in an extended $\beta$-strand conformation that lies 18 Å away from the PRL-1 active site (defined by the P-loop ($H^{103}CVAGLGR^{110}$)) and 20 Å from the C terminus of PRL-1 (Fig. 3*B*). Complex formation between PRL-1 and Peptide 1 buries a contiguous surface area of 1140 $Å^2$ in PRL-1.

The structure of the PRL-1·Peptide 1 complex defines a novel protein-protein interaction site in PRL-1 through an unexpected mode of interaction with the SH3 domain of p115 RhoGAP. The first three residues in Peptide 1 are invisible in the structure, and Ser-4 is exposed to solvent. Thus, interactions between PRL-1 and these residues, if present, are likely to be weak. Detailed interactions between PRL-1 and the rest of Peptide 1 are shown in Fig. 3*C*. Leu-5 in Peptide 1 is engaged in hydrophobic interactions with Asp-54 and Thr-56 in PRL-1. Ile-6 is within van der Waals contacts with Asp-54 and forms two weak polar interactions with the side chains of Asp-54 and Thr-55. Hydrophobic interactions are observed between Pro-7 in Peptide 1 and the side chain of Thr-55 and the phenyl ring of Try-53 in PRL-1. Pro-8 is also within van der Waals contacts with Thr-55. Both Lys-9 and Tyr-10 contact PRL-1 His-64. In addition, hydrophobic interactions exist between Tyr-10 and the side chains of Asp-67 and Trp-68, and Ile-11 may interact

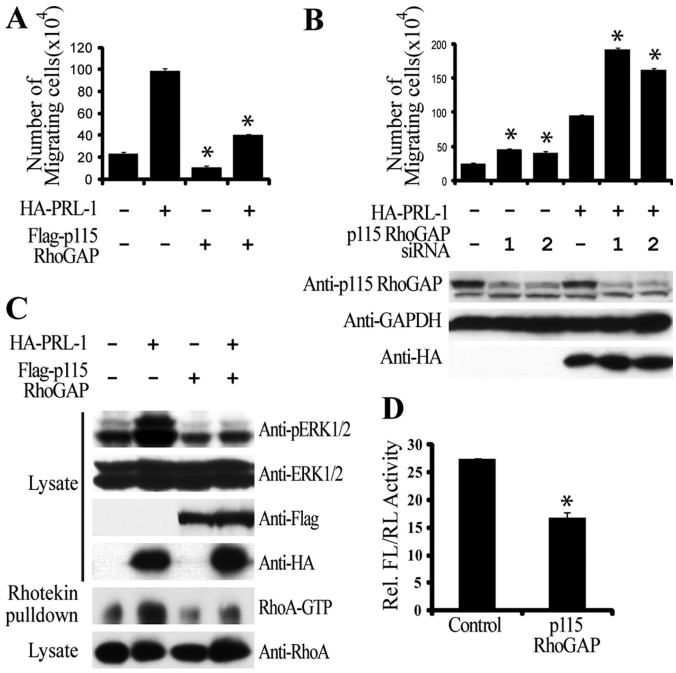


FIGURE 4. **p115 RhoGAP negatively regulates cell migration and ERK and RhoA activation.** *A*, overexpression of p115 RhoGAP inhibits cell migration in both control HEK293 cells and PRL-1-expressing HEK293 cells. *B*, knockdown of p115 RhoGAP enhances cell migration in both control HEK293 cells and PRL-1-expressing HEK293 cells. *C*, overexpression of p115 RhoGAP reduces ERK1/2 and RhoA activation in both control HEK293 cells and PRL-1-expressing HEK293 cells. *D*, p115 RhoGAP decreases RhoA-specific reporter activity. Results shown are representative of triplicate experiments with similar results. Results are presented as means ± S.D. *, $p < 0.01$. *Rel. FL/RL*, relative fluorescence/*Renilla* luciferase.

with Leu-66 and Trp-68. Finally, Thr-12 may form weak interactions with PRL-1 Trp-68 and Gln-79.

The residues within PRL-1 that are predicted to contact Peptide 1 from our structural data were probed for their requirement for interaction with both Peptide 1 and p115 RhoGAP. Serial truncations from either the N or C terminus of PRL-1 (full-length, 1–173) indicated that residues 1–120 and 30–173 still bound GST-Peptide 1, whereas fragments 1–90, 60–173, and 90–173 displayed no detectable binding (Fig. 3*D*). The results suggest that Peptide 1 likely binds within residues 30–120 in PRL-1. Additionally, the binding affinity of PRL-1 for Peptide 1 was significantly diminished when His-64 was replaced with Ala and completely abolished when Tyr-53 or Trp-68 was changed to Ala (Fig. 3*E*). Importantly, the latter two mutants also lacked the ability to immunoprecipitate p115 RhoGAP in HEK293 cells (Fig. 3*F*). These results are in complete agreement with the structural observations that the Tyr-53–Gln-79 sequence in PRL-1 is involved in binding Peptide 1. Importantly, residues within the Peptide 1-binding site are most likely also required for binding the analogous region within the SH3 domain of p115 RhoGAP.

Taken together, these results reveal a novel mode of interaction between an SH3 domain and its binding partner, where PRL-1 serves as the receptor for recognizing a sequence motif (corresponding to Peptide 1 Leu-5–Thr-12) within the SH3 domain of p115 RhoGAP. As shown in the crystal structure of the SrGAP1 SH3 domain (32), Pro-793 and Tyr-796 (Pro-7 and Tyr-10 in Peptide 1) form ligand-binding pocket 2, and Leu-791

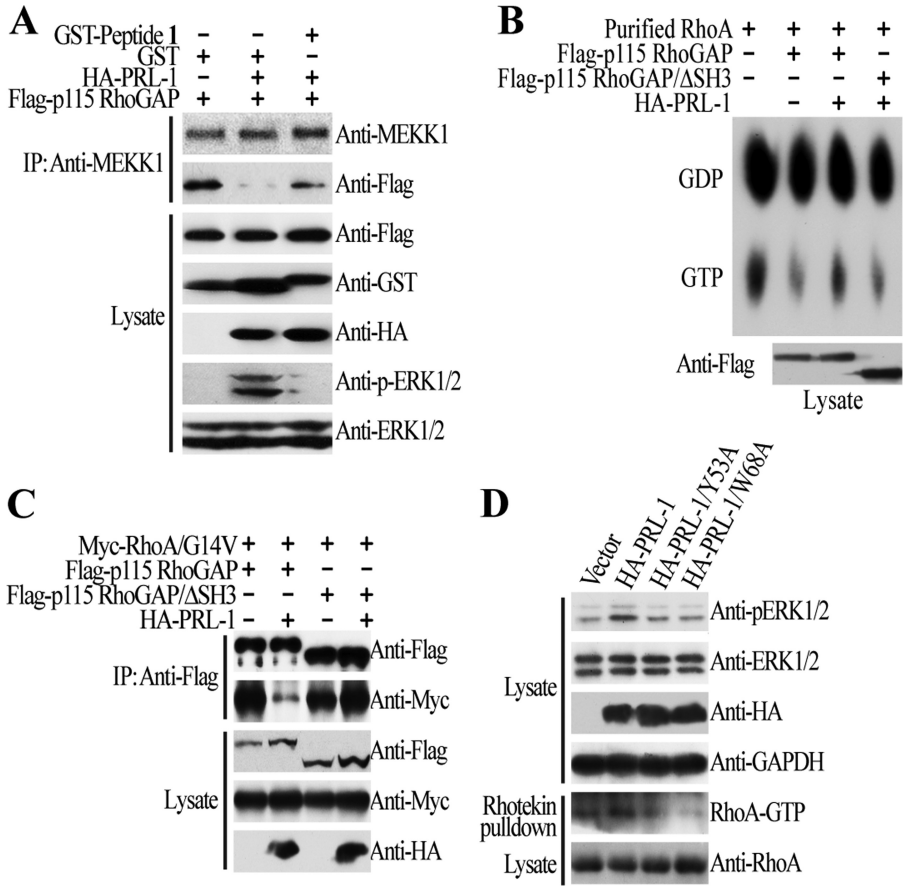


FIGURE 5. **Interaction between PRL-1 and p115 RhoGAP is responsible for PRL-1-mediated ERK1/2 and RhoA activation.** *A*, PRL-1 activates ERK1/2 by displacing MEKK1 from p115 RhoGAP. Control HEK293 cells and HA-PRL-1-expressing HEK293 cells were transfected with FLAG-tagged p115 RhoGAP with or without GST-Peptide 1. MEKK1 was immunoprecipitated (*IP*) with anti-MEKK1 antibody. The immunoprecipitates were blotted with anti-FLAG antibody to detect MEKK1-bound p115 RhoGAP. *B*, PRL-1 inhibits the GAP activity of p115 RhoGAP through its interaction with the SH3 domain of p115 RhoGAP. Immunoprecipitated FLAG-tagged p115 RhoGAP or p115 RhoGAPΔSH3 from either control HEK293 cells or HA-PRL-1-expressing HEK293 cells was incubated with purified GST-RhoA loaded with [$\alpha$-$^{32}$P]GTP. *C*, PRL-1 directly blocks the interaction between p115 RhoGAP and RhoA(G14V) in an SH3 domain-dependent manner. Control HEK293 cells and HA-PRL-1-expressing HEK293 cells were transfected with Myc-tagged RhoA(G14V) and FLAG-tagged p115 RhoGAP or p115 RhoGAPΔSH3. p115 RhoGAP and p115 RhoGAPΔSH3 were immunoprecipitated with anti-FLAG antibody. RhoA(G14V) associated with p115 RhoGAP or p115 RhoGAPΔSH3 was visualized with anti-Myc antibody. *D*, PRL-1-mediated ERK1/2 and RhoA activation requires physical interaction between PRL-1 and p115 RhoGAP. Substitution of Tyr-53 and Trp-68 in PRL-1 abrogated its ability to activate ERK and RhoA in HEK293 cells. Results shown are representative of triplicate experiments with similar results.

(Leu-5 in Peptide 1) lines ligand-binding pocket 3. Because there is no P*xx*P sequence in PRL-1 and because residues involved in binding Peptide 1 are noncontiguous (Fig. 3*C*), the recognition of Peptide 1 and the p115 RhoGAP SH3 domain by PRL-1 represents a novel protein-protein interaction, which differs from the canonical SH3 domain/P*xx*P-binding mode.

*p115 RhoGAP Negatively Regulates Cell Migration and ERK1/2 and RhoA Activation*—It is well documented that PRL-1 promotes cell migration through activation of the ERK1/2 and RhoA pathways (10, 11, 13, 14). It has also been reported that p115 RhoGAP inhibits cell motility through its GAP and C-terminal SH3 domains (31). To understand the functional significance of the novel interaction between PRL-1 and p115 RhoGAP, we evaluated the effect of modulating the expression of p115 RhoGAP on PRL-1-mediated cell migration as well as on ERK1/2 and RhoA activity. We found that overexpression of p115 RhoGAP in cells stably transfected with PRL-1 diminished PRL-1-induced cell migration (Fig. 4*A*). Overexpression of p115 RhoGAP in control cells also decreased basal migration, which is consistent with the previous report that p115 RhoGAP inhibits cell motility in NIH3T3 cells (31). In addition, p115 RhoGAP knockdown by siRNA enhanced cell migration in both control and PRL-1-expressing cells (Fig. 4*B*). Moreover, overexpression of p115 RhoGAP reduced PRL-1-mediated ERK1/2 and RhoA activation (Fig. 4*C*). Overexpression of p115 RhoGAP in control cells also reduced basal ERK and RhoA activity. The negative effect of p115 RhoGAP on RhoA signaling was further confirmed by a 40% decrease in the transcriptional activity of the RhoA-specific reporter SRE.L (Fig. 4*D*). We conclude that p115 RhoGAP plays a negative role in cell migration by down-regulating both ERK1/2 and RhoA activity.

*Mechanism of PRL-1-mediated ERK1/2 and RhoA Activation*—p115 RhoGAP has been previously found to associate with and inhibit MEKK1 through its SH3 domain (33). MEKK1 is the essential upstream kinase that phosphorylates and activates ERK1/2 and is required for cell motility. Because the region in the SH3 domain of p115 RhoGAP that corresponds to Leu-5–Thr-12 in Peptide 1 makes up the center of the P*xx*P ligand-binding site, PRL-1 binding to this site was pre-

dicted to block canonical interactions with this domain. We further speculated that one consequence of such displacement of MEKK1 from p115 RhoGAP by PRL-1 would be the activation of ERK1/2. To test this hypothesis, control and PRL-1-expressing cells were transfected with FLAG-tagged p115 RhoGAP, and the amount of p115 RhoGAP associated with MEKK1 and the phosphorylation status of ERK1/2 were measured. Compared with control cells, the fraction of p115 RhoGAP associated with MEKK1 was reduced, and the ratio of phosphorylated ERK1/2 was increased in PRL-1 cells (Fig. 5*A*). This effect is likely specific, as expression of GST-Peptide 1 restored the level of p115 RhoGAP associated with MEKK1 and concordantly reduced ERK1/2 phosphorylation (Fig. 5*A*). Thus, PRL-1 interaction with p115 RhoGAP likely mitigates the inhibitory effect of p115 RhoGAP on MEKK1, resulting in ERK1/2 activation.

Given that p115 RhoGAP inhibits RhoA by accelerating its catalysis of GTP hydrolysis to GDP (27, 33), we investigated whether PRL-1 binding to p115 RhoGAP could modulate its ability to regulate RhoA activity. To this end, immunoprecipitated FLAG-tagged p115 RhoGAP or p115 RhoGAPΔSH3 from either control or PRL-1 cells was incubated with purified GST-RhoA loaded with [$\alpha$-$^{32}$P]GTP. The data revealed that p115 RhoGAP from PRL-1 cells showed significantly lower GAP activity than that from control cells (Fig. 5*B*). This inhibitory effect of PRL-1 on p115 RhoGAP activity likely occurs via interaction with the SH3 domain, as p115 RhoGAPΔSH3 exhibited equal GAP activity in PRL-1-expressing or control cells (Fig. 5*B*). To further define the mechanism by which PRL-1 inhibits the GAP activity of p115 RhoGAP, we measured the effect of PRL-1 on the binding of p115 RhoGAP to RhoA(G14V), a constitutively active form of RhoA that stably associates with the GAPs due to resisting GTP hydrolysis. Control and PRL-1-expressing cells were transfected with Myc-RhoA(G14V) and FLAG-tagged p115 RhoGAP or p115 RhoGAPΔSH3. The amount of RhoA(G14V) associated with p115 RhoGAP or p115 RhoGAPΔSH3 was visualized by Western blotting. The observation that both full-length p115 RhoGAP and p115 RhoGAPΔSH3 bound RhoA(G14V) indicates that recognition of RhoA by p115 RhoGAP does not require its SH3 domain. In stark contrast, the ability of PRL-1 to block the interaction between RhoA(G14V) and p115 RhoGAP strongly depended on the presence of the SH3 domain (Fig. 5*C*). Apparently, the association of PRL-1 with the SH3 domain of p115 RhoGAP prevents p115 RhoGAP from binding RhoA, and this results in increased levels of GTP-bound RhoA. Finally, PRL-1 mutants PRL-1(Y53A) and PRL-1(W68A), which are defective in binding p115 RhoGAP, were unable to activate ERK1/2 or RhoA (Fig. 5*D*). This indicates that physical interaction between PRL-1 and p115 RhoGAP is a prerequisite for PRL-1-mediated ERK1/2 and RhoA activation.

In summary, starting from an unbiased screen for PRL-1 effectors, we have identified p115 RhoGAP as a *bona fide* PRL-1-binding protein. Biochemical and cellular studies suggested that the SH3 domain of p115 RhoGAP is required for its interaction with PRL-1. Structural analyses revealed that this interaction occurs via a novel protein-protein interaction whereby PRL-1 recognizes a conserved sequence motif in the canonical P*xx*P ligand-binding site of the SH3 domain in p115 RhoGAP. The interaction between PRL-1 and p115 RhoGAP coordinately activates the ERK1/2 pathway by displacing MEKK1 from p115 RhoGAP, and it activates RhoA by preventing its interaction with p115 RhoGAP. Our study not only offers a mechanistic explanation for ERK1/2 and RhoA activation by PRL-1 but also identifies a novel p115 RhoGAP-binding site in PRL-1 that can be used in the development of anticancer therapeutics by blocking the interaction between PRL-1 and p115 RhoGAP.

## REFERENCES


1. Diamond, R. H., Cressman, D. E., Laz, T. M., Abrams, C. S., and Taub, R. (1994) *Mol. Cell. Biol.* **14,** 3752–3762
2. Cates, C. A., Michael, R. L., Stayrook, K. R., Harvey, K. A., Burke, Y. D., Randall, S. K., Crowell, P. L., and Crowell, D. N. (1996) *Cancer Lett.* **110,** 49–55
3. Zeng, Q., Dong, J. M., Guo, K., Li, J., Tan, H. X., Koh, V., Pallen, C. J., Manser, E., and Hong, W. (2003) *Cancer Res.* **63,** 2716–2722
4. Zeng, Q., Si, X., Horstmann, H., Xu, Y., Hong, W., and Pallen, C. J. (2000) *J. Biol. Chem.* **275,** 21444–21452
5. Wang, J., Kirby, C. E., and Herbst, R. (2002) *J. Biol. Chem.* **277,** 46659–46668
6. Saha, S., Bardelli, A., Buckhaults, P., Velculescu, V. E., Rago, C., St Croix, B., Romans, K. E., Choti, M. A., Lengauer, C., Kinzler, K. W., and Vogelstein, B. (2001) *Science* **294,** 1343–1346
7. Stephens, B. J., Han, H., Gokhale, V., and Von Hoff, D. D. (2005) *Mol. Cancer Ther.* **4,** 1653–1661
8. Bessette, D. C., Qiu, D., and Pallen, C. J. (2008) *Cancer Metastasis Rev.* **27,** 231–252
9. Werner, S. R., Lee, P. A., DeCamp, M. W., Crowell, D. N., Randall, S. K., and Crowell, P. L. (2003) *Cancer Lett.* **202,** 201–211
10. Sun, J. P., Luo, Y., Yu, X., Wang, W. Q., Zhou, B., Liang, F., and Zhang, Z. Y. (2007) *J. Biol. Chem.* **282,** 29043–29051
11. Fiordalisi, J. J., Keller, P. J., and Cox, A. D. (2006) *Cancer Res.* **66,** 3153–3161
12. Achiwa, H., and Lazo, J. S. (2007) *Cancer Res.* **67,** 643–650
13. Luo, Y., Liang, F., and Zhang, Z. Y. (2009) *Biochemistry* **48,** 1838–1846
14. Nakashima, M., and Lazo, J. S. (2010) *J. Pharmacol. Exp. Ther.* **334,** 627–633
15. Roux, P. P., and Blenis, J. (2004) *Microbiol. Mol. Biol. Rev.* **68,** 320–344
16. Hall, A. (1998) *Science* **279,** 509–514
17. Bishop, A. L., and Hall, A. (2000) *Biochem. J.* **348,** 241–255
18. Bollag, G., and McCormick, F. (1995) *Methods Enzymol.* **255,** 161–170
19. Quilliam, L. A., Rebhun, J. F., Zong, H., and Castro, A. F. (2001) *Methods Enzymol.* **333,** 187–202
20. Wells, C. D., Gutowski, S., Bollag, G., and Sternweis, P. C. (2001) *J. Biol. Chem.* **276,** 28897–28905
21. Otwinowski, Z., and Minor, W. (1997) *Methods Enzymol.* **276,** 307–326
22. Navaza, J. (1994) *Acta Crystallogr. A* **50,** 157–163
23. Sun, J. P., Wang, W. Q., Yang, H., Liu, S., Liang, F., Fedorov, A. A., Almo, S. C., and Zhang, Z. Y. (2005) *Biochemistry* **44,** 12009–12021
24. Brünger, A. T., Adams, P. D., Clore, G. M., DeLano, W. L., Gros, P., Grosse-Kunstleve, R. W., Jiang, J. S., Kuszewski, J., Nilges, M., Pannu, N. S., Read, R. J., Rice, L. M., Simonson, T., Warren, and G. L. (1998) *Acta Crystallogr. D* **54**, 905–921
25. Brünger, A. T. (1992) *Nature* **355,** 472–475
26. Jones, T. A., Zou, J. Y., Cowan, S. W., and Kjeldgaard, G. J. (1991) *Acta Crystallogr. A* **47**, 110–119
27. Tribioli, C., Droetto, S., Bione, S., Cesareni, G., Torrisi, M. R., Lotti, L. V., Lanfrancone, L., Toniolo, D., and Pelicci, P. (1996) *Proc. Natl. Acad. Sci. U.S.A.* **93,** 695–699
28. Wong, K., Ren, X. R., Huang, Y. Z., Xie, Y., Liu, G., Saito, H., Tang, H.,

Wen, L., Brady-Kalnay, S. M., Mei, L., Wu, J. Y., Xiong, W. C., and Rao, Y. (2001) *Cell* **107,** 209–221
29. Soderling, S. H., Binns, K. L., Wayman, G. A., Davee, S. M., Ong, S. H., Pawson, T., and Scott, J. D. (2002) *Nat. Cell Biol.* **4,** 970–975
30. Tcherkezian, J., and Lamarche-Vane, N. (2007) *Biol. Cell* **99,** 67–86
31. Vogt, D. L., Gray, C. D., Young, W. S., 3rd, Orellana, S. A., and Malouf, A. T. (2007) *Mol. Cell. Neurosci.* **36,** 332–342
32. Li, X., Chen, Y., Liu, Y., Gao, J., Gao, F., Bartlam, M., Wu, J. Y., and Rao, Z. (2006) *J. Biol. Chem.* **281,** 28430–28437
33. Christerson, L. B., Gallagher, E., Vanderbilt, C. A., Whitehurst, A. W., Wells, C., Kazempour, R., Sternweis, P. C., and Cobb, M. H. (2002) *J. Cell. Physiol.* **192,** 200–208